

## Gas Density Dynamics in Pulsed Interelectrode Discharge Trace

© M.E. Renev, Yu.V. Dobrov, V.A. Lashkov, I.Ch. Mashek, R.S. Khoronzhuk

St. Petersburg State University,  
199034 St. Petersburg, Russia  
e-mail: renevme@mail.ru

Received January 25, 2024

Revised March 18, 2024

Accepted March 18, 2024

We present a numerical investigation into the dynamic processes governing the formation of a rarefied region in air at pressures of 10.7 and 101.3 kPa, maintained at temperature of 300 K, influenced by plasma heating from an interelectrode microsecond discharge. Experimental validation of our computational findings was conducted specifically for a pressure of 101.3 kPa. Our estimations reveal a remarkable agreement between the experimentally measured nested energy value of  $57 \pm 6$  mJ and our numerical prediction, which stands at approximately 58 mJ. We observed a significant spatiotemporal congruence in the medium density distribution. Within the interelectrode gap, the gas density diminishes to 0.1 times its initial value within a time frame of  $3 \mu\text{s}$ , predominantly due to the formation of radially expanding flow zones. Notably, gas density experiences a more rapid decline near the electrodes, attributed to the higher local specific heating power and the consequent emergence of near-electrode shock waves.

**Keywords:** validation, plasma, simulation, air, energy deposition.

DOI: 10.61011/TP.2024.05.58518.20-24

### Introduction

During last two decades for aerodynamics improvement and control of flow around the aircrafts moving with speed significantly higher the sound speed the plasma technologies of flight control are developed [1–4]. Their use ensure low-inertia control of oncoming flow movement during possible decrease in resistance and thermal loads. The plasma generators use different technologies to form plasma of required type (hot and unbalanced, bulk or surface etc.), having own applications. Such devices have a potential for use on aircrafts where common mechanized systems of flight control practically reach limit of modernization possibility [5].

The particular interest is applied to the problem of reducing thermal and mechanical loads of different bodies (blunt, wedge-shaped, etc.) during significant supersonic flow around, which nonlinearly increase with Mach number increasing [2]. One of the options to solve these problems is organization of gas local heating in supersonic flow before the body, which results in dynamic restructuring of the shock wave, decreasing of resistance and heat flows [1–4,6–11].

The paper [9] shows that local density heterogeneity in the oncoming supersonic flow near the cylindrical body results in short-time decreasing of pressure in critical point to 40%, and of heat flows — to 15%.

Papers [6–8] relate to the numerical analysis of the effect of external heating, flow gas non-equilibrium on the supersonic flow around of the blunt body, drag coefficient. It is shown that we can decrease stagnation pressure by two times, if we use extended local heating in supersonic flow

approaching the body. At that the thinner the heating area with fixed added energy is the higher the degree of effect and effectiveness of such method are.

In papers [6–10,12–17] the numerical simulation was used to analyze the effect of energy deposition on gas-dynamic phenomena caused by it. Equations of gas dynamics of equilibrium gas with specified energy deposition were solved without review of the plasma dynamics. Under such approach to the numerical simulation we obtain data on the principle opportunity to control the gas flows and accompanying phenomena. At the same time it is important to know how optimally, from the point of view of the necessary effect on the gas-dynamic flow, convert the electric energy into the plasma formation with necessary parameters.

In papers [18–20] the numerical simulation of the energy deposition was made considering the plasma dynamics, when the energy deposition depends on the set electrical parameters, geometry, medium etc. Such coordinated calculations are technically complex and require significant computing resources. To exclude said difficulties in current paper we suggest a two-stage model of microsecond spark electrode discharge in air, intended for approximate analysis of a rarefied region formation caused by plasma heating. Systems of equations of plasma and gas dynamics are solved separately at the first and second stages, respectively. Based on the obtained plasma parameters the heating power is calculated, it is set by specific way when solving gas-dynamic stage in form of external source. Validation of the suggested method of numerical simulation is performed: the calculation results are compared with experimental data.

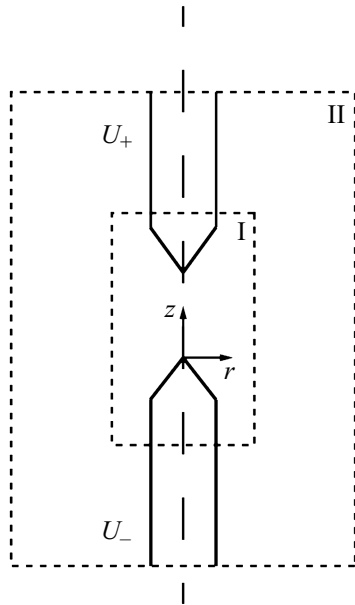


**Figure 1.** Geometry of model (axisymmetric): cathode ( $U_-$ ), anode ( $U_+$ ), I — region of simulation for first stage, II — region of simulation of second stage (includes I), dashed borders of regions — open borders.

## 1. Numerical simulation

The following conditions of formation of pulse spark electrode discharge are considered. Voltage generator forms a rectangular unipolar pulse with amplitude 20 kV, pulse width 3  $\mu$ s, width of leading and trailing edges — 200 ns. The voltage is applied to electrodes via ballast resistor 800  $\Omega$ . Distance between electrodes — 6 mm. Medium — air. Two coaxial copper sharpened electrodes are used. Calculations were performed for gas pressures 10.7 and 101.3 kPa. Geometry of region of calculation is shown in Fig. 1, axisymmetric two-dimensional setting.

### 1.1. Objective setting at first stage of simulation

At first stage the system of equations of plasma dynamics is solved in region I to determine heating power distribution not considering the gas dynamic phenomena. The region I is selected such that its dimensions will be sufficient to describe the interelectrode discharge: further increase in dimensions of the region of calculation does not result in obvious change of the results. The system of equations for the electrode discharge is used, it is shown in [20–22]: Poisson–Nernst–Planck equations and equations for energy of electron gas. Additionally we considered voltage drop in electrodes power supply circuit.

$$U = U_0(T) - IR, \quad (1)$$

$$-\varepsilon_0 \Delta \varphi = \rho_{ch}, \quad \rho_{ch} = |e|(n_+ - n_e - n_-), \quad \mathbf{E} \equiv -\nabla \varphi, \quad (2)$$

$$\frac{\partial n_e}{\partial t} + \nabla \mathbf{J}_e = S_e, \quad \mathbf{J}_e \equiv -b_e \mathbf{E} n_e - \nabla D_e n_e, \quad (3)$$

$$\frac{\partial n_e \psi}{\partial t} + \nabla \mathbf{J}_\psi + (\mathbf{E}, \mathbf{J}_e) = I^i S^i, \quad \mathbf{J}_\psi \equiv -b_e \mathbf{E} n_e \psi - \nabla D_e n_e \psi, \quad (4)$$

$$\rho_g = \frac{\partial \omega_i}{\partial t} = \nabla \rho_g \omega_i \mathbf{V}_i + S_i,$$

$$\mathbf{v}_i \equiv D_i \nabla (\ln \omega_i + \ln M_g) + \frac{D_i^T}{\rho_g \omega_i} \nabla \ln T_g - z_i b_i \mathbf{E}, \quad (5)$$

where  $U$  — voltage on electrodes,  $U_0(t)$  — power supply voltage,  $I$  — electric current,  $R$  — electric resistance of power circuit,  $\varepsilon_0$  — electric constant,  $\varphi$  — electric potential,  $\rho_{ch}$  — density of bulk charge,  $|e|$  — elementary charge;  $n_e, n_+, n_-$  — bulk concentrations of electrons, positive and negative ions, respectively,  $\mathbf{E}$  — electric field strength vector,  $\mathbf{J}_e$  and  $\mathbf{J}_\psi$  — densities of flows of electrons and electron energy, respectively,  $S_e$  — source of electrons,  $S_i$  — source of components of  $i$ -grade,  $I^i$  and  $S^i$  — potential of threshold reaction  $i$  and its speed,  $b_e$  and  $b_i$  — electron and ion mobility coefficients,  $D_e$  and  $D_i$  — diffusion coefficients of electrons and ions,  $\psi$  — average energy of one electron,  $\rho_g$  — medium density,  $\omega_i$  — mass fraction of  $i$ -component,  $\mathbf{V}_i$  — movement speed vector of  $i$ -component,  $M_g$  — average molar mass,  $z_i$  — charge number.

Electrons and heavy components are considered:  $O_2, O_2(\alpha 1\Delta), O_2^-, O_2^+, N_2, N_2(A), N_2(a), N_2^+, O, O^-, O^+, N, N^+, NO, NO^+$ . Reactions of impact ionization of heavy components by electrons and reactions of excitation of all components were taken from [23–27], at that transitions to new states were not considered. Such approach is widespread and allows for more accurate calculation of the electron gas temperature and, hence, all reactions with their participation without model complication. Exclusion is three metastable states —  $O_2(\alpha 1\Delta), N_2(A), N_2(a)$ , which formation speed were calculated. Adhesion reactions are introduced for oxygen containing components, detachment from the atom and molecule of oxygen was considered [23–27]. Recombination reactions electron–ion and ion–ion are taken from [28,29]. The association reactions of neutral components are taken from the article [30].

In considered model the cathode is earthed, electrical potential is applied to the anode, the potential is equal to power supply voltage:

$$\varphi_1 = 0, \quad \varphi_2 = U. \quad (6)$$

Flows of electrons and electron energy via the metal surface are sum of the following flows. Electrons can pass free from the medium into the metal due to drift (under action of the electric field, first term) and heat motion (second term), reverse flow is determined by the expression for emission of electrons by ions (third term). When the electron is absorbed by the anode the electron gas losses the energy: the kinetic energy of one electron and potential energy (pressure of electron gas decreases). Appropriate limit conditions:

$$\mathbf{J}_e \Big|_{1,2} = -b_e n_e (\mathbf{E}, \mathbf{n}) \Theta(\mathbf{E}, \mathbf{n}) \Big|_{1,2} - \frac{1}{2} v_e^{th} \mathbf{n} \Big|_{1,2} - \sum_i \gamma_i \mathbf{J}_i \Big|_{1,2}, \quad (7)$$

$$\mathbf{J}_\psi|_{1,2} = -b_e n_e \psi(\mathbf{E}, \mathbf{n}) \Theta(\mathbf{E}, \mathbf{n})|_{1,2} - \frac{5}{6} v_e^{th} \mathbf{n}|_{1,2} - \sum_i \gamma_i W_i \mathbf{J}_i|_{1,2}, \quad (8)$$

where  $\mathbf{n}$  — normal of surface—interfaces medium—electrode is oriented inside the electrode,  $\Theta(x)$  — Heaviside theta function equal to 1 at  $x > 0$  and equal to 0 at  $x < 0$ ,  $\gamma_i$  — coefficient of secondary ion-electron emission for  $i$ -grade of ion,  $W_i$  — energy of ions emitted  $i$ -grade of electron,  $v_e^{th}$  — speed of thermal movement of electrons.

Ions are neutralized on surface of electrodes with reaction rate  $S_i^{surf}$ , there is flow of ions on electrode:

$$\mathbf{J}_i|_{1,2} = -S_i^{surf} \mathbf{n}|_{1,2}. \quad (9)$$

At the initial time moment there is small seed concentration of electrons  $10^{13} \text{ m}^{-3}$  and equal to it concentration of positive ions, electrodes are not charged.

## 1.2. Objective setting at second stage of simulation

At second stage the gas dynamics is calculated with set energy input for region II as per results of the first stage of simulation. Region II increasing as compared to region I is necessary to calculate dynamics of the gas disturbed by plasma heating in the interelectrode region. To describe the compressed medium (air, perfect gas) the system of Navier–Stokes equations is solved using the approach RANS considering turbulence (model  $k-\varepsilon$ ) and considering heat transfer by thermal conductivity, convection with external energy deposition. The desired values: density, medium pressure, two speed components, temperature, kinetic energy of turbulence, rate of dissipation of turbulence kinetic energy, turbulent viscosity (8 values). Total number of equations and definitions is equal to 8.

On surfaces of cathode and anode the adhesion conditions are set, on open border of region II constant pressure and temperature of undisturbed medium are set. Dimensions of region II are selected such that do not affect the dynamics of processes near the discharge trace.

The specific power of the energy input was calculated at second stage as follows. Based on results of simulation the power of plasma heating  $W_{HEAT}^0$  (zero approximation):

$$W_{HEAT}^0 = \sum_i (\mathbf{J}_i, \mathbf{E}) + \sum_j S_j \Delta H_j, \quad (10)$$

where  $\Delta H_j$  — enthalpy jump during a reaction  $j$ .

All Joule heatings by partial currents of individual grades of ions (first term) and energy releases during reactions (second term) are summed up.

Based on  $W_{HEAT}^0$  the corrected value  $W_{HEAT}^{corr}$  is introduced for the situation of resistor presence in power circuit, on the resistor the major portion of voltage drops at significant plasma current. Correction has no time delay. Plasma during time period about 10 ns is adjusted for the changed conditions: voltage on electrodes, pressure, medium temperature. The characteristic time of gas dynamic processes

is much larger. But it is necessary to consider the effect of these processes as plasma electrical resistance, Joule heating directly depend on them.

Let's review the law of charge conservation for one-dimensional case (axis  $z$ ) for some region where the density of medium, through which the set current passes, will change.

$$\frac{\partial \rho_{ch}}{\partial t} + \frac{\partial J_z}{\partial z} = 0, \quad (11)$$

where  $J_z$  — current density along axis  $z$ . As in the discharge the charge relaxation occurs very quick in relation to the gas dynamic processes (about 10–100 ns against units  $\mu\text{s}$ ), the we can disregard the partial derivative of charge density with respect to time. Then we obtain that along axis  $z$  the current density shall be a constant value.

Mobility of electrons is higher then mobility of ions, by two orders of magnitude, so they almost completely determine the current in low-temperature plasma, intensively gain energy and introduce it into the medium via inelastic reactions. Current projection

$$J_z = -|e| \left( b_e n_e E_z - D_e \frac{\partial n_e}{\partial z} + V_{g_z} n_e \right). \quad (12)$$

First current component — drift, along axis  $z$  it is proportional to the mobility of electrons and strength of the electric field  $E_z$ . Second component — diffusion current of electrons proportional to diffusion constant and concentration gradient. Third component — convection transport, along the axis  $z$  proportional to speed of medium  $V_{g_z}$ .

Current density in plasma is determined, first of all, by the drift component — first component. For example, at voltage on the electrodes of 1 kV, and interelectrode gap length of 6 mm the characteristic value of the field strength in the plasma channel is equal to 1.6 kV/cm. At atmospheric pressure the mobility of electrons is about  $0.04 \text{ m}^2/(\text{V}\cdot\text{s})$ . In this case the speed of the drift movement of electrons is 4 km/s. The convection flows at the medium speed 330 m/s will distort the total value of current by 8% only, so their effect can be neglected. The diffusion current is assumed low, as in other case significant gradients of electron concentrations will be necessary, but this is not observed in the plasma channel during spark discharge. In such case the formula is simplified to

$$J_z = -|e| b_e n_e E_z. \quad (13)$$

The medium heating by plasma  $W_{HEAT}^{corr}$  results in its expansion. Inside the heated region the medium density, its resistance, and, hence, heating will decrease. The mobility of electrons increases inversely proportional to the density of the medium. After medium density decreasing the electric field shall proportionally decrease. Expression for  $W_{HEAT}^{corr}$ :

$$W_{HEAT}^{corr} = J_z E_z = J_z E_z^0 \frac{N_g}{N_g^0} = \frac{N_g}{N_g^0} W_{HEAT}^0. \quad (14)$$

Statement on predominance of the electron component of the plasma current of interelectrode discharge is true for

the region not containing near-electrode layers. Near them the electron concentrations decrease by many times. The derivation of the corrected power of heating by ion currents is similar, since the electric field strength increases near the electrodes, and as before, the drift flows of the particles in question prevail over the convection and diffusion flows.

The current density during time period of voltage pulse action changes weakly at developed spark discharge and the power circuit comprises the external resistor. In experiment performed in the present paper we obtained currents about 24.0–24.5 A at power circuit resistance 800  $\Omega$  and power voltage 20 kV. Voltage on electrodes decreases from 800 to 400 V by two times. Current increases by 0.5 A (2%) only. So, we suppose that upon power correction the current density  $J_z$  is constant.

The specific power of plasma heating  $W_{HEAT}^{corr}$  is applied for time of voltage pulse during calculation of the second gas dynamic stage of gas dynamics in interelectrode space.

### 1.3. Package of numerical simulation, grid for two stages of simulation

For numerical study we used package Comsol Multi-Physics, ensuring numerical study of the electrical dynamics, plasma, gas dynamics. Modules „Plasma“, „Nonisothermal flow“ were used. The second module is module for compressed medium calculation with heat transfer. Grid for the first stage: near the electrodes the layers of ordered rectangular grid (from 10 nm to 10  $\mu$ m, 500 layers in total 800  $\mu$ m), the rest space — triangular free grid (maximum element size 400  $\mu$ m, growth rate no more than 1.1). Grid for the second stage: the basis is grid of the first stage and is being completed in new region (free triangular, maximum element size 0.4 mm).

### 1.4. Numerical simulation results

The calculation results showed that with pressure increasing from 10.7 and 101.3 kPa the plasma channel width becomes lower: narrowing from 1 to 0.25 mm. The specific heating power is also redistributed. Fig. 2 shows distribution of specific bulk power of medium heating by the discharge along axis  $z$ . It is evident that at pressure 10.7 kPa the interelectrode gap in the middle is heated quicker ( $10^{13}$  W/kg) than at 101.3 kPa ( $10^{12}$  W/kg): the reduced heating power is by order of magnitude greater. Near the cathode values of the specific heating power are equal to  $10^{16}$  and  $2 \cdot 10^{16}$  W/kg for 10.7 and 101.3 kPa respectively, and near anode —  $6 \cdot 10^{13}$  and  $4 \cdot 10^{14}$  W/kg.

Fig. 3 shows spatial distributions of medium density for time moments 350 ns, 1 and 5  $\mu$ s. The formation of two near-electrode waves is visible, they come from the ends of the cathode and anode. At 350 ns the distance from them to electrodes is 0.5 mm. At 350 ns there is no region of decreased pressure, in rest part of the interelectrode gap the zone of radially expanding flow is absent.

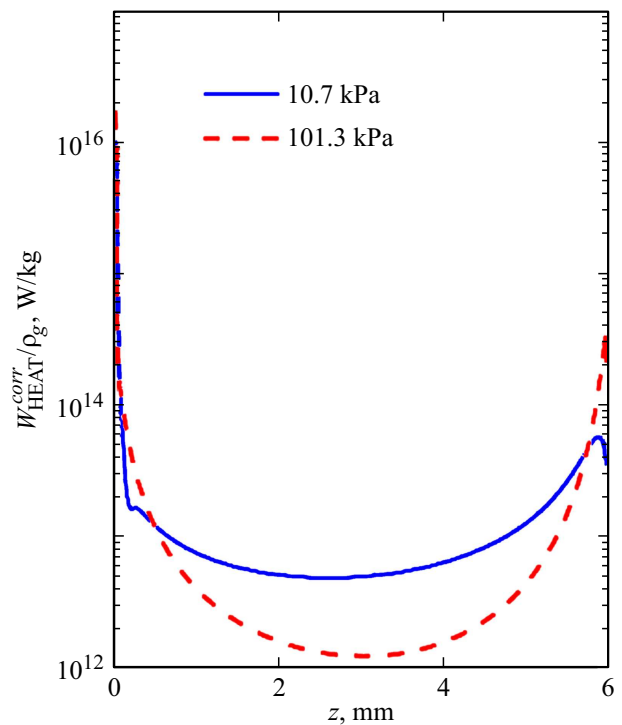


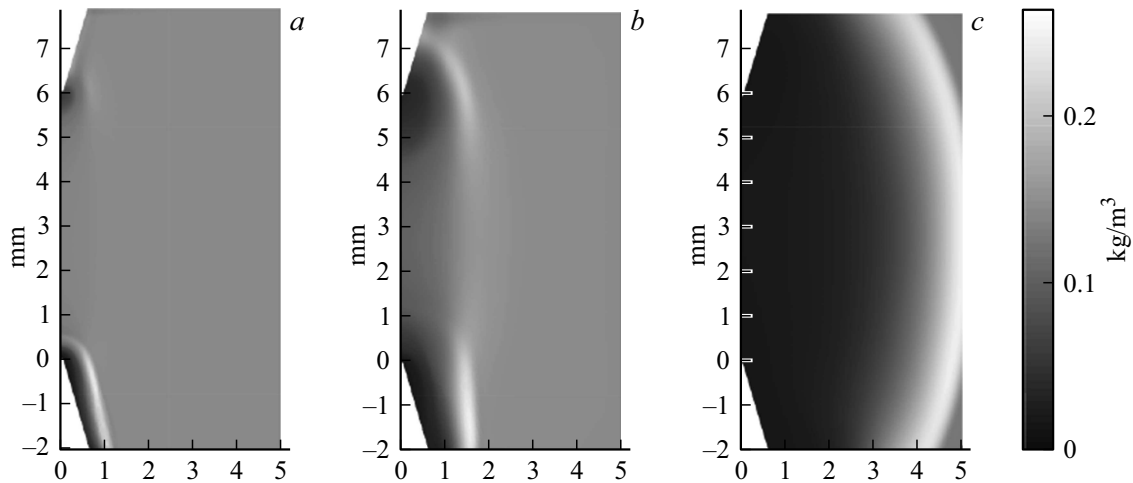
**Figure 2.** Distribution of specific bulk power of medium heating by discharges along axis  $z$  for pressures 10.7 and 101.3 kPa.

After 350 ns the zone of radially expanding flow is created. At time 1  $\mu$ s two previously formed near-electrode waves disappear practically completely: there are no their borders with increased density. At time 5  $\mu$ s the zone of radially expanding flow significantly (up to 10 times) decreases the medium density in interelectrode gap.

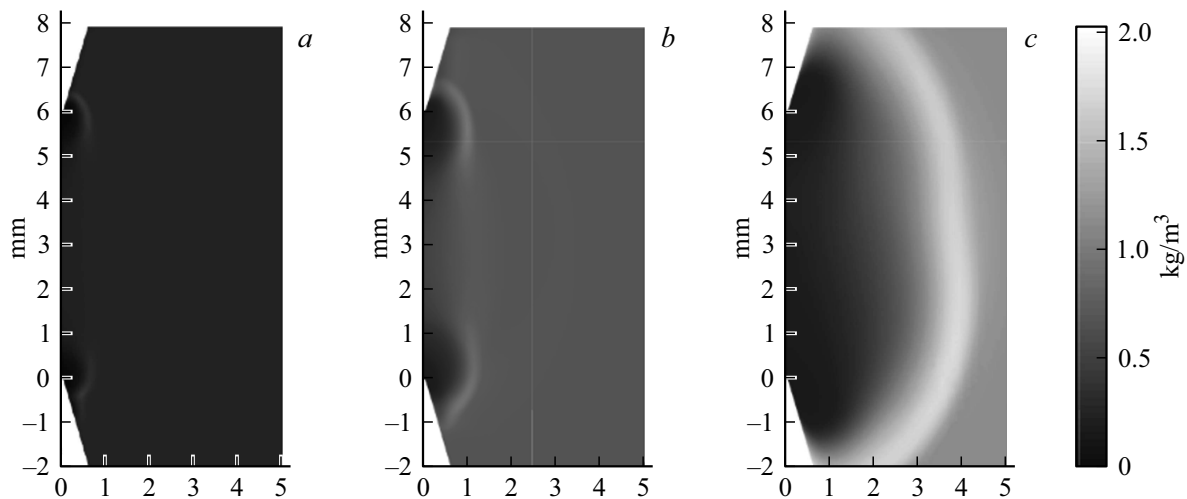
Fig. 4 shows similar graphs for pressures 101.3 kPa and time moments 500 ns, 1 and 5  $\mu$ s. As compared with the case of pressure 10.7 kPa there is more intensive formation of the near-electrode waves and their slow merging into the zone of radial expanding flow. Only at time moment 500 ns its formation starts, and at time moment 3  $\mu$ s merging of near-electrode waves completes.

Fig. 5 shows graphs of medium density distribution along axis  $z$  (Fig. 5, *a*) and along axis  $r$  ( $z = 3$  mm, Fig. 5, *b*). The near-cathode heating is rather powerful: at 100 ns the shock wave coming from the cathode already present.

Shock wave quickly weakens: at 350 ns it becomes a simple compression wave. Density jump due to wave also decreases. Near anode the acoustic wave is formed as the specific heating power is by two orders of magnitude lower. At time moment 350 ns density decreasing in the middle of gap starts. At this time the near-electrode waves don't have time to reach the middle of the gap, hence, they can not affect the formation of zone of radially expanding flow. At time 1  $\mu$ s this zone has obvious influence on the medium density: behind the wave it decreases by several times, and is increased before the wave. On the discharge axis the density decreases by up to 10 times at time 5  $\mu$ s.



**Figure 3.** Distribution of gas density at initial pressure 10.7 kPa: *a* — 350 ns, *b* — 1, *c* — 5  $\mu$ s.



**Figure 4.** Distribution of gas density at initial pressure 101.3 kPa: *a* — 500 ns, *b* — 1, *c* — 5  $\mu$ s.

The calculation shows that the near-electrode waves result in medium pressure oscillations along the discharge axis. Fig. 6 shows graphs of pressure spatial distribution along axis  $z$  and  $r$ . Pressure at 100 ns in gap 1–5 mm increases by 5 times, and near electrodes — by up to 12–15 times. After 500 ns there is pressure force directed to electrodes near their surface. At 1  $\mu$ s in entire gap the pressure difference is observed resulting in medium movement to surface of electrodes.

Fig. 7 shows distributions of medium movement speed. They show speed profile of shock wave (600 m/s behind the shock wave front, and before wave there is medium at rest having sound speed maximum 410 m/s), coming from the cathode at time moment 100 ns. At the same time from anode the acoustic wave spreads with speed about 60 m/s. At time moment 350 ns temperatures 650 K are achieved on discharge axis due to plasma heating, the sound speed increases to 500 m/s. The shock wave as it moves away from the cathode it slows down and becomes acoustic wave, at

time moment 350 ns its movement speed achieved 300 m/s. The acoustic wave coming from anode increases its speed to 150 m/s. At time moment 500 ns movement in reverse direction towards electrodes occurs, and two discussed waves slow down. At 1  $\mu$ s regions of reverse movement to electrodes with speed up to 300 m/s are clearly visible, they at 3  $\mu$ s together occupy the entire interelectrode gap. The zone of radially expanding flow (Fig. 7, *b*) at 500 ns has movement speed 120 m/s and continues acceleration. Behind it the medium at 3  $\mu$ s moves with speed exceeding sound speed of the undisturbed medium, the shock wave is formed.

At pressure 101.3 kPa the dynamics of waves formation is similar to case of pressure 10.7 kPa. The differences are slow formation of the zone of radially expanding flow (by 150 ns later) and in more intensive near-electrode waves. The first difference is associated with lower value of specific heating in region of gap middle. The second difference — discharge energy deposition more localized at surface of electrodes.

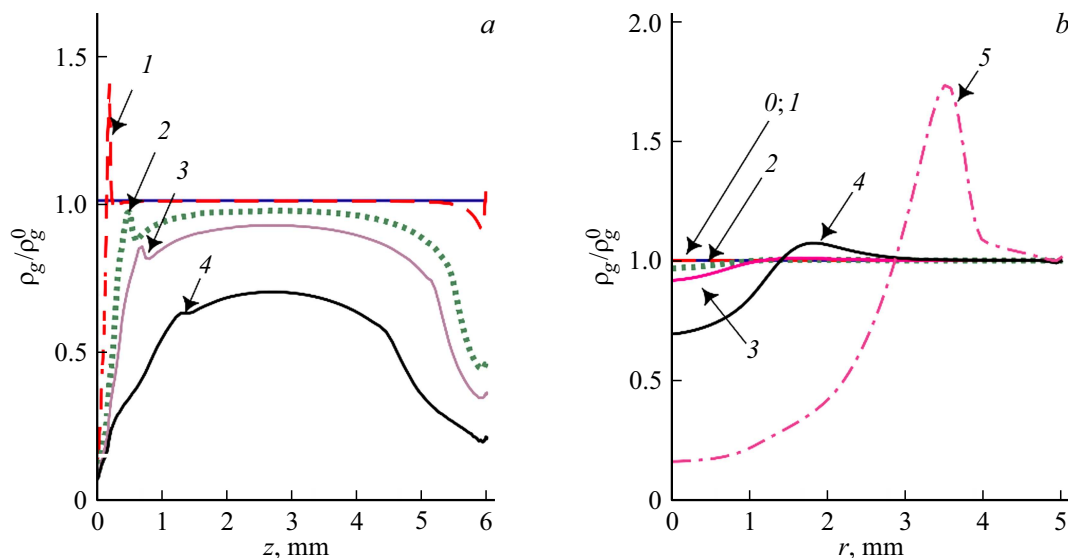


**Figure 5.** Spatial distribution of the medium density normalized to the initial value (10.7 kPa) along axes: *a* — axis *z*, *b* — axis *r* (*z* = 3 mm). Time moments: 0 — initial, 1 — 100, 2 — 350, 3 — 500 ns, 4 — 1, 5 — 3  $\mu$ s.

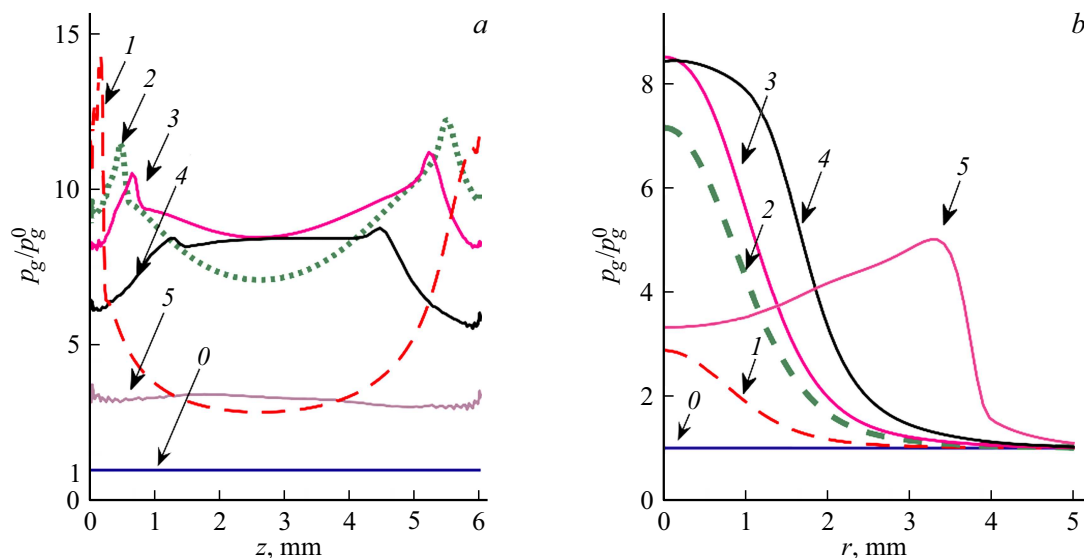


**Figure 6.** Spatial distribution of the medium pressure normalized to the initial value (10.7 kPa) along axes: *a* — axis *z*, *b* — axis *r* (*z* = 3 mm). Time moments: 0 — initial, 1 — 100, 2 — 350, 3 — 500 ns, 4 — 1, 5 — 3  $\mu$ s.

## 2. Experiment

### 2.1. Experiment setting

The experiment was performed at medium (air) pressure of 101.3 kPa. The system of electrodes shown in Fig. 8 was used. The parameters of medium and electric voltage are same as during numerical calculation. Cathode and anode — copper needles with diameter of 2 mm (sharpening — 0.5 mm), interelectrode distance is 6 mm. The pulse interelectrode discharge is performed, applied voltage is 20 kV, ballast resistor 800  $\Omega$ , pulse width is 3  $\mu$ s. Wedge is manufactured using 3D-printing from ABS-plastic, face surface of wedge has dimensions 15  $\times$  20 mm.

The gas-dynamic processes were visualized using the shadow diagram involving device IAB-451 [31]. Fig. 8 shows the experiment scheme. The shadow photos were registered as follows: light beam from source 1 passes through the limiting slit on the mirror 2, then is directed on the spherical mirror 3 and, after reflection passes through inclined lens 4. Then the parallel light beam passes through the work part of the aerodynamic tube 5 and optical system comprising inclined lens 4, spherical mirror 3, diagonal mirror 2. Then the light flow passes through Foucault knife 6 located in beam focus, and enters the eyepiece of observation tube 7.

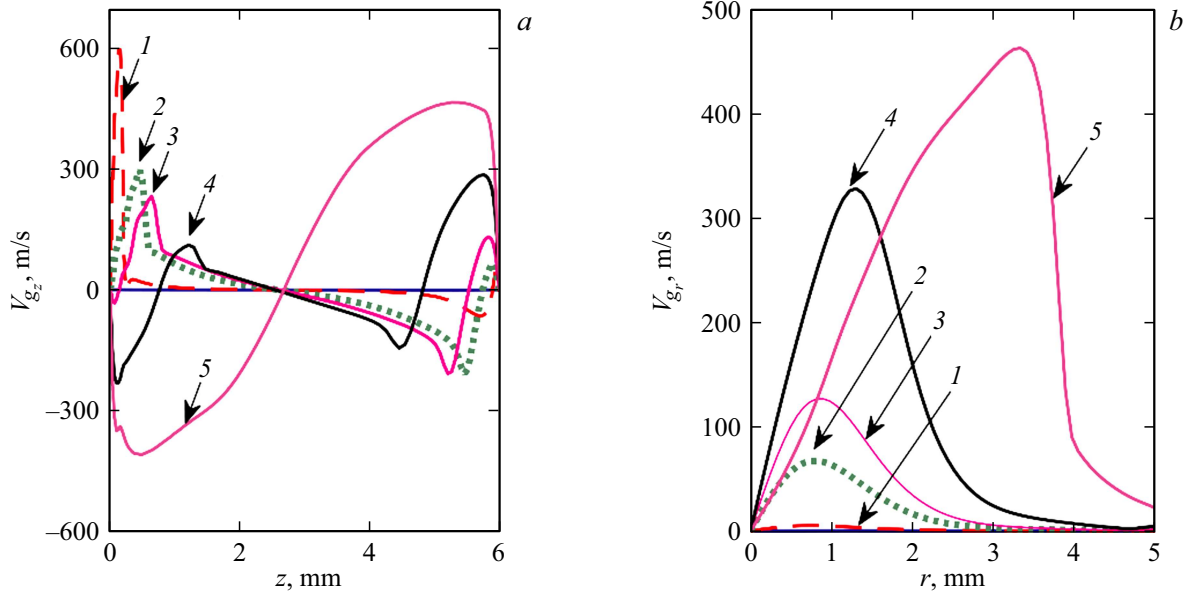


**Figure 7.** Spatial distribution of medium movement speed (10.7 kPa) along axes: *a* — axis *z*, *b* — axis *r* (*z* = 3 mm). Time moments: 1 — 100, 2 — 350, 3 — 500 ns, 4 — 1, 5 — 3 μs.

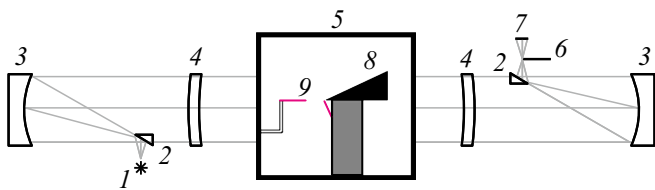


**Figure 8.** Schematic image of Tepler shadow device IAB-451, 1 — light source, 2 — mirror, 3 — spherical mirror, 4 — beveled lens, 5 — work part of aerodynamic tube, 6 — Foucault knife, 7 — eyepiece of the observation system, 8 — model secured on holder, 9 — electrodes.

Inside the work part the electrode attached to the holder are located. Between electrodes the distance 6 mm is maintained, and electrode thickness is 2 mm with sharpening at ends. Changing the Foucault knife we can adjust the intensity of screen illumination. Tepler optical device can register disturbances, such as, compression shock waves and expansion shock waves that arise in the flow. Tepler device backlight is ensured using LED lamp with luminous efficiency 50 Lm/W.

Images were registered using camera „Basler avA1000-100gm“ with the shortest frame exposure time equal to 12 μs. To acquire the experimental data the software LabView running on platform NI-USB 6343 was used. Discharge burning voltage was registered by a digital oscilloscope „Hantek DSO-4084C“ using high voltage divider.

**2.2. Experimental results**

Fig. 9, *a* shows the shadow photo of the discharge trace for time moment 5 μs. Edge of Foucault knife was set

parallel to discharge development path. It is obvious that at this time moment there is visible discharge trace: region of decreased density surrounded by thin dark region. The wave with axial symmetry and form close to cylindrical form is identified.

For comparison with numerical simulation the field of gradient of coefficient of light refraction in the radial direction relative to the trace is rotated such that the trace is vertical. Next the section is plotted from center of trace to the undisturbed medium perpendicular to the trace. Integration is performed with a variable limit (from the second point of the section, different number of pixels) of the brightness of the photo pixels. The obtained dependence of integral value on path length in pixels is converted in the dependences of medium density on radius. For this the integral values are normalized, and constant value (undisturbed medium density) is added. Normalization is selected until the necessary level of medium density is obtained. Pixels number conversion into distance is performed by known number of pixels between the needle edges. So, the medium density restored based on shadow photo can be compared by position of maximum of medium density.

Comparison of the experimental results and numerical simulation shows satisfactory matching. Fig. 9, *b* shows distributions of medium density along axis *r* from numerical calculation and restored one. At time moment 5 μs the zone of radially expanding flow was obtained in both study methods. Positions of density maxima, obtained experimentally and by calculations, coincide.

Medium density restored by photo near the trace axis was not compared according to following reasons. The shadow method is based on change of the refraction index

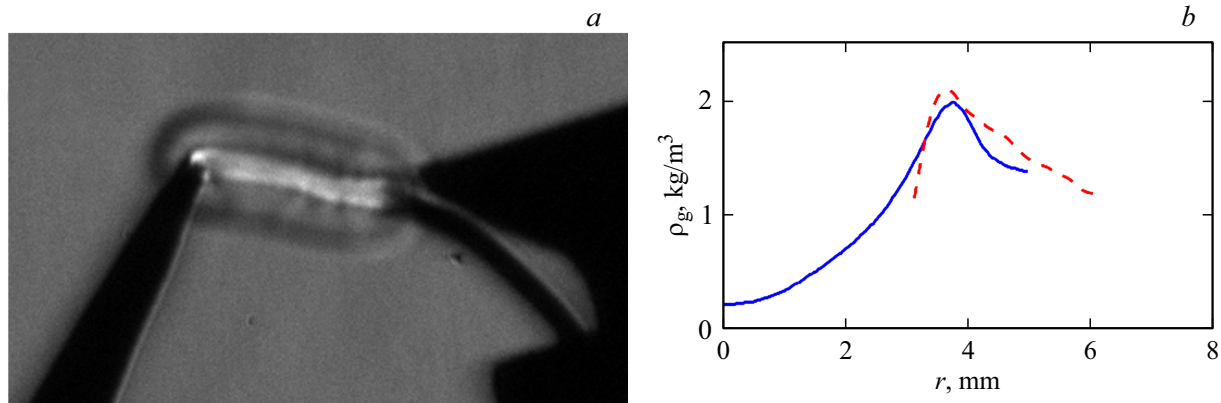


**Figure 9.** Validation of numerical model, time moment  $5\mu\text{s}$ , pressure 101.3 kPa: *a* — shadow pattern photo, experiment, *b* — density distribution along radius: numerical calculation (solid line) and experiment (dashed line).

depending also on other not considered factors, for example, medium temperature. Near the axis the density is rather high, non-physical. The electrode system in the experiment consumed  $57 \pm 6\text{ mJ}$  to form one spark discharge, value was calculated by dependences of current and voltage on time. The total power of Joule heating and the time integral of it were experimentally calculated. After results obtaining of numerical simulation the integral of (14) over space and time. As result we obtained that thermal energy nested in the medium is 58 mJ.

## Conclusion

Numerical and experimental studies were performed on dynamics of thermal expansion waves caused by pulse electrode discharge (20 kV) at medium pressures 10.7 and 101.3 kPa at currents below 25 A. The satisfactory agreement was obtained between the results of numerical and experimental analyses: the magnitude of energy deposition, the size of the zone of radially expanding flow.

The suggested model has some simplifications, such as separate solution of equations of plasma dynamics in medium at rest, gas dynamics with the external heating (by plasma). When solving equations of gas dynamics we use new approximate description of the external heating by medium density. The model ensures more quicker data acquisition on dynamic of the medium density, temperature, medium movement and formation of shock, acoustic waves as compared to the case of calculations using the matched models.

The model shows that upon start of plasma heating by the spark discharge first of all near-electrode waves (100–350 ns) are formed. The zone of radially expanding flow occurs at 350 ns. At  $5\mu\text{s}$  it become shock one and results in medium density decreasing by up to 10 times.

Thus, as a result of the experimental and numerical study, it was shown that it is possible to use the considered approach for approximate simulation of the gas density dynamics after energy deposition by plasma, but further

the model validation is required for the case of different medium pressures.

## Funding

Numerical study of plasma dynamics in gas at rest was financed by grant № 22-1-1-17-4 of Fund of Development of Theoretical Physics and Mathematics „BASIS“; numerical simulation of gas dynamics with given energy supply, and experimental studies were carried out financed by grant from the Russian Science Foundation № 23-19-00241.

## Conflict of interest

The authors declare that they have no conflict of interest.

## References

- [1] V.M. Fomin, P.K. Tretyakov, J.P. Taran. *Aerospace Sci. Technol.*, **8** (5), 411 (2004). DOI: 10.1016/j.ast.2004.01.005
- [2] P. Bletzinger, B.N. Ganguly, D.V. Wie, A. Garscadden. *J. Phys. D: Appl. Phys.*, **38** (4), R33 (2005). DOI: 10.1088/0022-3727/38/4/R01
- [3] A. Russell, H. Zare-Behtash, K. Kontis. *J. Electrostat.*, **80**, 34 (2016). DOI: 10.1016/j.elstat.2016.01.004
- [4] A.Y. Starikovskiy, N.L. Aleksandrov. *Plasma Phys. Reports*, **47** (2), 148 (2021). DOI: 10.1134/S1063780X21020069
- [5] A.F. Latypov, V.M. Fomin. *J. Appl. Mech. Tech. Phys.*, **43** (1), 59 (2002).
- [6] O.A. Azarova. *Aerospace*, **2** (1), 118 (2015). DOI: 10.3390/aerospace2010118
- [7] O.A. Azarova, V.G. Grudnitsky, Y.F. Kolesnichenko. *Matem. Mod.*, **18** (1), 79 (2006).
- [8] O.A. Azarova, A.V. Erofeev, T.A. Lapushkina. *Tech. Phys. Lett.*, **43** (4), 405 (2017). DOI: 10.1134/S1063785017040150
- [9] Y.V. Dobrov, V.A. Lashkov, I.Ch. Mashek, R.S. Khoronzhuk. *AIP Conference Proceedings* (SPb., Russia, 2018), v. 1959, N 1, p. 050009. DOI: 10.1063/1.5034637

- [10] Y.V. Dobrov, M.E. Renev, V.A. Lashkov, I.Ch. Mashek, R.S. Khoronzhuk. *J. Phys.: Conf. Ser.*, **1959** (1), 012016 (2021). DOI: 10.1088/1742-6596/1959/1/012016
- [11] V.A. Lashkov, A.G. Karpenko, R.S. Khoronzhuk, I.Ch. Mashek. *Phys. Plasmas*, **23** (5), 052305 (2016). DOI: 10.1063/1.4949524
- [12] A.A. Firsov, E. Dolgov, S.B. Leonov. *AIAA Scitech 2019 Forum* (San Diego, California, 2019), DOI: 10.2514/6.2019-0739
- [13] P.Yu. Georgievskij, V.A. Levin. *Pis'ma v ZhTF*, **14** (8), 684 (1988). (in Russian)
- [14] P.Yu. Georgievskij, V.A. Levin. *Tr. MIAN SSSR*, **186**, 197 (1989). (in Russian).
- [15] P.Yu. Georgievskij. *Vestnik Nizhegorodskogo un-ta im. N.I. Lobachevskogo*, **4** (3), 711 (2011). (in Russian).
- [16] N. Kianvashrad, D.D. Knight. *J. Phys. D: Appl. Phys.*, **52** (49), 494005 (2019). DOI: 10.1088/1361-6463/ab3fb6
- [17] O. Azarova, D.D. Knight, Y. Kolesnichenko. *48th AIAA Aerospace Sciences Meeting Including the New Horizons Forum and Aerospace Exposition* (Orlando, Florida, 2010)
- [18] A.I. Saifutdinov, E.V. Kustova, A.G. Karpenko, V.A. Lashkov. *Plasma Phys. Rep.*, **45** (6), 602 (2019). DOI: 10.1134/S1063780X19050106
- [19] N.A. Popov. *Plasma Phys. Rep.*, **32** (3), 237 (2006). DOI: 10.1134/S1063780X06030068
- [20] T. Piskin, V.A. Podolsky, S.O. Macheret, J. Poggie. *J. Phys. D: Appl. Phys.*, **52** (30), 304002 (2019). DOI: 10.1088/1361-6463/ab1fbc
- [21] N.S.J. Braithwaite. *Plasma Sources Sci. Technol.*, **9** (4), 517 (2000).
- [22] A.I. Saifutdinov, E.V. Kustova. *J. Appl. Phys.*, **129** (2), 023301 (2021). DOI: 10.1063/5.0031020
- [23] Electronic resource. *Biagi database*. Access mode: [www.lxcat.net](http://www.lxcat.net) (retrieved on October 28, 2021).
- [24] Electronic resource. *IST-Lisbon database*. Access mode: [www.lxcat.net](http://www.lxcat.net) (retrieved on October 28, 2021).
- [25] Electronic resource. *Morgan database*. Access mode: [www.lxcat.net](http://www.lxcat.net) (retrieved on October 28, 2021).
- [26] Electronic resource. *FLINDERS database*. Access mode: [www.lxcat.net](http://www.lxcat.net) (retrieved on October 28, 2021).
- [27] Electronic resource. *Itikawa database*. Access mode: [www.lxcat.net](http://www.lxcat.net) (retrieved on October 28, 2021).
- [28] Yu.P. Rajzer. *Fizika gazovogo razryada* (Intellekt, Dolgoprudny, 2009), s. 736. (in Russian).
- [29] C. Lazarou, A.S. Chiper, C. Anastassiou, I. Topala, I. Mihaila, V. Pohoata, G.E. Georghiou. *J. Phys. D: Appl. Phys.*, **52** (19), 195203 (2019). DOI: 10.1088/1361-6463/ab06cd
- [30] C. Park, J.T. Howe, R.L. Jaffe, G.V. Candler. *J. Thermophys. Heat Transfer*, **8** (1), 9 (1994). DOI: 10.2514/3.496
- [31] L.A. Vasil'ev. *Tenevye metody* (Nauka, Glavnaya red. Fizmatlit, M., 1968), s. 400. (in Russian)

*Translated by IMazurov*